Low-Loss Multilayered Metamaterial Exhibiting a Negative Index of Refraction at Visible Wavelengths

Carlos García-Meca,* Juan Hurtado, Javier Martí, and Alejandro Martínez
Nanophotonics Technology Center (NTC), Universidad Politécnica de Valencia, Camino de Vera s/n, 46022, Valencia, Spain

Wayne Dickson and Anatoly V. Zayats
Nano-optics and Near-field Spectroscopy Laboratory, Department of Physics, King's College London, Strand, London WC2R 2LS, United Kingdom

(Received 22 October 2010; revised manuscript received 7 January 2011; published 11 February 2011)

We experimentally demonstrate a low-loss multilayered metamaterial exhibiting a double-negative refractive index in the visible spectral range. To this end, we exploit a second-order magnetic resonance of the so-called fishnet structure. The low-loss nature of the employed magnetic resonance, together with the effect of the interacting adjacent layers, results in a figure of merit as high as 3.34. A wide spectral range of negative index is achieved, covering the wavelength region between 620 and 806 nm with only two different designs.

DOI: 10.1103/PhysRevLett.106.067402 PACS numbers: 78.20.Ci, 42.25.Bs

Optical media with a negative index of refraction are theoretically allowed by Maxwell's laws of electromagnetism [1]. Although not found in natural materials, a negative refraction index has been successfully achieved using artificial nanostructured materials termed metamaterials [2]. The interest in negative index media (NIM) lies in the importance of their exceptional properties, such as the possibility of superlensing or light storing [3,4]. Metamaterials exhibiting a negative index of refraction have been experimentally demonstrated in several ranges of the electromagnetic spectrum [2,5]. However, it is in the visible regime where we can take full advantage of NIM properties. For instance, the superior imaging ability of NIMs would be essential for visible microscopy, with applications in microelectronics, bio- and nanotechnology.

The desired features for a NIM are low loss and isotropy. This last property includes by itself some other features such as polarization independence and negative-index behavior in the three spatial directions. The strict condition to obtain a negative real part of the refractive index $n = n' + in''$ is $\varepsilon''\mu' + \mu''\varepsilon' < 0$ [6], where the permittivity and permeability are $\varepsilon = \varepsilon' + i\varepsilon''$ and $\mu = \mu' + i\mu''$, respectively. Therefore, a NIM having negative ε' and μ', called double-negative NIM, is required if low losses are demanded. Up to now, only in a few experiments have negative index metamaterials been demonstrated in the visible spectrum, and none of the above features have been attained [7–9]. Although a large part of the visible spectrum has been covered by the nanofabricated NIMs (wavelengths from 580 to 780 nm), the current challenge is to improve the above-mentioned aspect in order to make these metamaterials suitable for practical applications.

In this work, we have fabricated multilayer NIMs that exhibit double-negative behavior at visible wavelengths while presenting low-loss and polarization independent optical properties at normal incidence. This has been achieved by exploiting the properties of a second-order magnetic resonance of the so-called fishnet structure, in contrast to previous works that used first-order magnetic resonances, both related to gap surface plasmon polariton (SPP) Bloch modes. Moreover, the fabricated metamaterial is the first experimental NIM in the visible regime made up of several unit cells along the propagation direction, an important step towards bulk NIMs in this band.

The recent experimental demonstrations of NIMs in the visible range are based on different variations of the so-called fishnet metamaterial [7–9] (see Fig. 1), which consists of $2N + 1$ alternating metal (m) and dielectric (d)

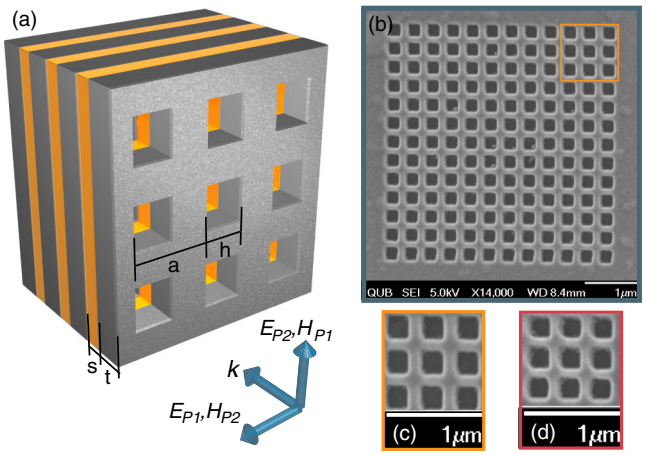

FIG. 1 (color online). (a) Schematic of a fishnet metamaterial made up of three unit cells in the propagation direction. The overall number of layers is 7 (4 metal layers and 3 dielectric layers). (b) Top-view SEM image of the fabricated 3-unit-cell fishnet structure 3 (see Table I). (c) Detail of image in (b). (d) Detail of the fabricated 3-unit-cell fishnet structure 4.

stacked hole arrays resulting in N metamaterial unit cells in the propagation direction ($N = 1$ corresponds to *m-d-m*, $N = 2$ to *m-d-m-d-m*, ...). This structure can be described by an effective permittivity governed by the cutoff frequency of the waveguide mode supported by the holes despite wavelength-scale nanostructuring [10,11]. The negative index of this structure arises from the combination of this effective negative permittivity with the permeability resonance resulting from the excitation of a gap SPP in the metal-dielectric-metal multilayer [10–12]. Since the multilayered structure is periodically patterned and forms a plasmonic crystal, its SPP Bloch modes can be excited at certain frequencies when diffraction of light on the periodic structure contributes towards matching the wave vectors of SPP and photons [13–15].

In all recent experimental realizations, the fishnet negative index is a consequence of the excitation of the first-order SPP Bloch mode along the Γ-X direction of the Brillouin zone of the square lattice crystal. The main drawback of this approach is the high loss due to the weak nature of this resonance in the employed configurations. For instance, in experiments [7–9], the maximum figure of merit (FOM), which is a standard loss measure defined as FOM $= |n'/n''|$, is 0.5, 0.7, and 0.3, respectively, implying large absorption losses. Theoretical analysis reveals that the use of SPP Bloch modes in the Γ-M direction of the Brillouin zone (the so-called second order magnetic resonance) makes attainable a strong permeability resonance with an associated negative permeability within the negative permittivity region [16]. In the overlapping band, the structure exhibits a double-negative refractive index with low loss. One of the fundamental advantages of this structure is that the square lattice structure leads to polarization insensitive optical properties at normal incidence. Although there are ways to improve the loss aspect in fishnet structures based on the first-order SPP resonance [17], it has been shown that, for a polarization independent configuration, the FOM associated with the second-order resonance is noticeably higher than that of the first-order one. Thus, the use of the second-order resonance is more adequate if our goal is to achieve low-loss and polarization independence simultaneously. It is worth mentioning that polarization independence has not been attained in previous experiments, either due to the geometry of the employed structures (based on nonsquare holes or lattices) or to fabrication limitations.

Another issue is the transition from two-dimensional to bulk metamaterial behavior in this geometry. It is known that the constitutive parameters of the fishnet metamaterial change with an increasing number of functional layers, until they stabilize for a certain N [16,18]. Moreover, the addition of more layers in this metamaterial also enhances the FOM [16,18,19]. Thus, the fabrication of a multiple-functional-layer fishnet metamaterial is highly desirable. Given the previous considerations, we designed several seven-layer ($N = 3$) fishnet structures with the second order magnetic resonance in the visible spectral range. Structures with a single functional layer were investigated for comparison (see Table I). It is worth stressing that only single-layer fishnet structures with negative index in the visible spectrum had been fabricated until now.

The designed structures with several sets of parameters (Table I) were fabricated as follows. Soda lime glass (refractive index of 1.51) was used as a bulk substrate. Silver layers of thickness t were deposited by e-beam evaporation at 2.5 Å $\cdot$ s^{-1}. Spin-on resist FOX-12 (provided by Dow Corning) based on hydrogen silsesquioxane (HSQ) was used as the interlayer dielectric. The resist was diluted in methyl isobutyl ketone in a ratio of 1:6 and spinned at 6000 rpm with an acceleration of 3000 rpm $\cdot$ s^{-1}. It was annealed after deposition to remove solvents and densify the film. The resulting refractive index of the dielectric layers (thickness s) in the considered spectral range was 1.41. An additional HSQ layer of the same thickness was deposited on top of the outer silver layer to avoid environmental effects. Thus, the one- and three-unit-cell structures were made up of four and eight layers, respectively. To create the periodic pattern of square holes, focused ion-beam milling was used due to its ability to achieve high aspect ratio geometries. Geometrical patterns were designed on a pixel-by-pixel basis, with each point represented by its spatial coordinate (specifying ion-beam position) and an associated dwell time controlling the milling duration. Initially, depth calibration was performed using atomic force microscope characterization of structures fabricated with a range of milling times. Lateral dimensions were adjusted using scanning electron microscope (SEM) data to ensure ion-beam tail effects were incorporated in the final designs. The ion current used for all fabrication was maintained at a maximum of 10 pA, ensuring the smallest focused spot size, at an accelerating voltage of 30 kV. Top-view SEM images of some of the fabricated structures are shown in Fig. 1.

Experimental and simulated spectra of the fabricated metamaterials are presented in Fig. 2. Numerical modeling was performed with CST Microwave Studio. In the simulations, silver was characterized by a Drude-Lorentz model including a term accounting for interband transitions [20]. The adjustable parameters α (chosen such that the collision frequency $\gamma_c = 8.5 \times 10^{13}$ s^{-1}) and β were set to match experimental data. Note that, due to the interband transitions term, the losses ascribed to Ag are somewhat

TABLE I. Geometrical parameters of the fabricated structures.

Structure	N	Ag layers	HSQ layers	t (nm)	s (nm)	h (nm)	a (nm)
1	1	2	2	35	30	250	400
2	1	2	2	35	30	220	365
3	3	4	4	35	15	250	400
4	3	4	4	35	15	220	350

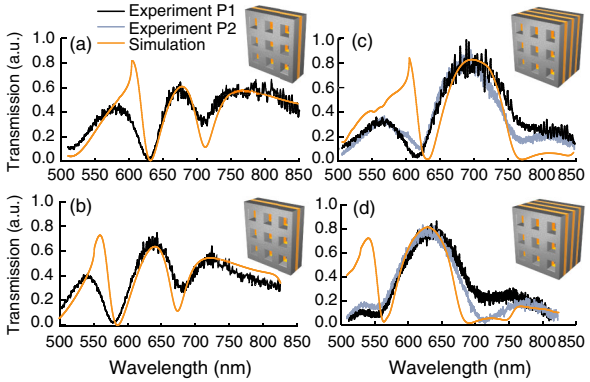

FIG. 2 (color online). Normal incidence zero-order measured and simulated transmission spectra of different fabricated metamaterials: (a) structure 1 (see Table I), (b) structure 2, (c) structure 3, and (d) structure 4. Polarization of the incident light with respect to the crystal lattice is shown in Fig. 1.

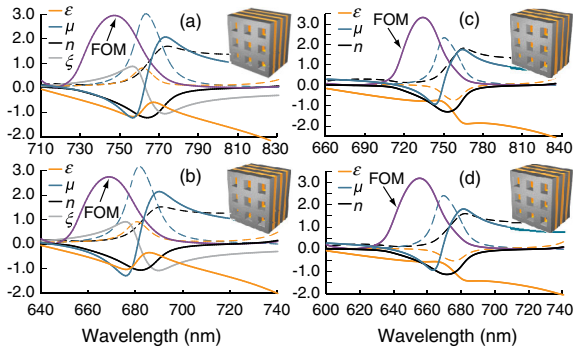

FIG. 3 (color online). FOM and real (solid) and imaginary (dashed) parts of the fabricated structures effective parameters with [(a) structure 3 and (b) structure 4] and without [(c) structure 3 and (d) structure 4] the substrate and top HSQ layer. $\xi = \xi' + i\xi''$ is the bianisotropy parameter.

higher than in previous works. The optical transmission spectra were measured using a fiber-coupled spectrometer with a liquid-nitrogen-cooled CCD and W-halogen white-light source. The normal incidence transmission spectra are the same (within fabrication tolerances) for the two orthogonal polarizations of the incident light along the main axes of the crystal lattice, which confirms the polarization independence at normal incidence. A good agreement between the simulations and the measurements is observed, verifying the reliability of the numerical results, from which the effective metamaterial parameters can be extracted. Discrepancies at short wavelengths below Wood's anomaly (dips around 600 nm) are due to the fact that only zero-order transmission is captured in the measurements, while total transmission is calculated in the simulations, including high-order diffraction beams. A generalized version of the retrieval algorithm described in [21] was used to account for the bianisotropy introduced by the substrate and top HSQ layer. The retrieved parameters of the fabricated structures with $N = 3$ are shown in Fig. 3, where we also depict the retrieved parameters for the free-standing case to allow for comparison with previous works where bianisotropy was not considered (note that the fabricated structures were optimized for the free-standing case). Results are very similar in both cases. The main features of all the fabricated metamaterials are summarized in Table II together with the data for the other experimentally made metamaterials for the free-standing case. As can be seen, a high FOM with a maximum value of 1.9 is observed in the 1-functional-layer structures. The spectral ranges covered by the NIM region in these metamaterials span 656–712 nm (structure 1) and 620–672 nm (structure 2). A further improvement of the figure of merit is achieved with the 3-functional-layer structure, reaching values as high as 3.34. In this case, the NIM spectral ranges are 693–806 (structure 3) and 620–713 nm (structure 4). A minimum negative index of -1.3 is achieved (structure 3), with a FOM $= 2.73$ at the wavelength at which $n = -1$. It is worth mentioning that the ratio of the free space wavelength to the size of the unit cell along the propagation direction goes from 12.4 to 15.6. It has been shown that the zeroth-order Bloch mode dominates propagation inside a fishnet structure so that it can be considered as homogeneous [22]. An indicator of this property is the convergence of the refractive index with increasing N, which has been verified for the fishnet configuration used here at $N \sim 8$ [16]. Nevertheless, the optical properties of the fabricated

TABLE II. Main features of fabricated metamaterials in comparison with previous experiments. The numbers in parenthesis in column 1 refer to the corresponding structure in Table I. The polarization independence column refers only to the case of normal incidence.

Reference	N	min (n')	max (FOM)	$n < 0$ bands	Polarization independent	Double negative
[7]	1	−0.6 (780 nm)	0.5 (780 nm)	~750–800 nm	No	No
[8]	1	−1 (776 nm)	0.7 (772 nm)	753–810 nm	No	No
[9]	1	−0.25 (580 nm)	0.3 (580 nm)	567–602 nm	No	No
This work (1)	1	−0.68 (690 nm)	1.9 (678 nm)	656–712 nm	Yes	Yes
This work (2)	1	−0.66 (650 nm)	1.75 (642 nm)	620–672 nm	Yes	Yes
This work (3)	3	−1.3 (752 nm)	3.34 (734 nm)	694–806 nm	Yes	Yes
This work (4)	3	−1.13 (670 nm)	3.19 (655 nm)	620–713 nm	Yes	Yes

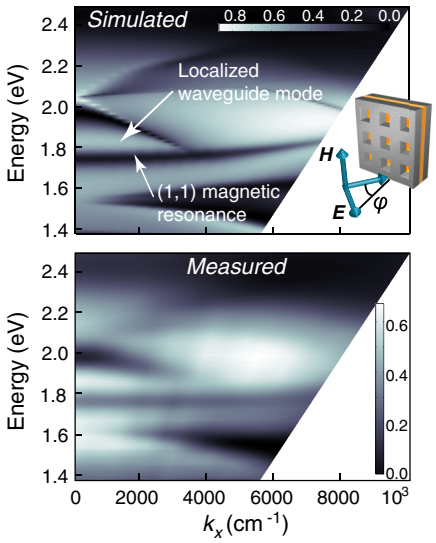

FIG. 4 (color online). Simulated and measured transmission of structure 1 as a function of transverse wave vector and photon energy. The incident light is *p* polarized with respect the plane of incidence. The response is similar for *s* polarized light (not shown).

structures have been optimized for their specific number of unit cells.

The angular dependence of the optical properties of the fabricated metamaterials has also been studied. The transmission dispersion measurements were performed in the angular range of 0°–30°, showing a very good agreement between simulations and experiment (Fig. 4). The main physical phenomena involved in the creation of the double-negative band can be observed in the dispersion plot. On one side, the wide transmission band around 1.86 eV (667 nm) can be identified with the localized resonance occurring at the cutoff frequency of the waveguide mode supported by the holes (see also Fig. 2). This mode controls the effective permittivity of the metamaterial [11]. On the other side, the forbidden band observed approximately at 1.75 eV (708 nm), corresponds to the SPP in the Γ-*M* direction of the Brillouin zone, which is responsible for the permeability resonance. Remarkably, the SPP Bloch modes corresponding to this resonance exhibit weak dispersion, in contrast to the highly dispersive SPP modes supported by unstructured metal-dielectric-metal multilayers or previous typical fishnet configurations. This may be ascribed to the large size of the apertures compared to the unit cell size and the hybridization of the SPP mode with the above-mentioned localized resonance [10]. The flatness of the SPP band responsible for the magnetic resonance suggests the possibility to achieve nearly angle-independent NIM properties in a considerable angular range.

It is worth mentioning that by using an active optical medium as the dielectric layer and under optical pumping conditions it becomes feasible to overcome losses and even achieve gain in a fishnet metamaterial [23]. In this sense, our metamaterial is merely passive and its performance could be much improved by making use of an active optical medium in the wavelength region at which the negative-index behavior is obtained.

In conclusion, we have experimentally characterized multilayer fishnet metamaterials with simultaneously negative permittivity and permeability in the visible regime. This entails an important step towards homogeneous NIMs in this spectral range. The metamaterial exhibits low losses and polarization independence at normal incidence. In addition, it has been found that the gap-SPP Bloch modes determining the permeability resonance display weak dispersion. Further refinement of the fabrication process is expected to extend the negative-index band towards shorter wavelengths.

Financial support by the Spanish MICINN (Contracts No. CSD2008-00066 and No. TEC2008-06871-C02) and by the Valencian government (Contract No. PROMETEO-2010-087) is acknowledged. C. G.-M. acknowledges financial support from Grant FPU of MICINN. W. D. and A. Z. acknowledge financial support from EPSRC (U.K.).

*To whom correspondence should be addressed.
cargarm2@ntc.upv.es

[1] V. G. Veselago, Sov. Phys. Usp. **10**, 509 (1968).
[2] R. A. Shelby, D. R. Smith, and S. Schultz, Science **292**, 77 (2001).
[3] J. B. Pendry, Phys. Rev. Lett. **85**, 3966 (2000).
[4] K. L. Tsakmakidis, A. D. Boardman, and O. Hess, Nature (London) **450**, 397 (2007).
[5] C. M. Soukoulis, S. Linden, and M. Wegener, Science **315**, 47 (2007).
[6] R. A. Depine and A. Lakhtakia, Microw. Opt. Technol. Lett. **41**, 315 (2004).
[7] G. Dolling, M. Wegener, C. M. Soukoulis, and S. Linden, Opt. Lett. **32**, 53 (2007).
[8] U. K. Chettiar *et al.*, Opt. Lett. **32**, 1671 (2007).
[9] S. Xiao *et al.*, Opt. Lett. **34**, 3478 (2009).
[10] A. Mary *et al.*, Phys. Rev. Lett. **101**, 103902 (2008).
[11] C. García-Meca *et al.*, Opt. Express **17**, 6026 (2009).
[12] R. Ortuño *et al.*, Phys. Rev. B **79**, 075425 (2009).
[13] A. V. Zayats, I. I. Smolyaninov, and A. A. Maradudin, Phys. Rep. **408**, 131 (2005).
[14] W. Dickson, G. A. Wurtz, P. R. Evans, R. J. Pollard, and A. V. Zayats, Nano Lett. **8**, 281 (2008).
[15] A. Minovich *et al.*, Phys. Rev. B **81**, 115109 (2010).
[16] C. García-Meca *et al.*, Opt. Lett. **34**, 1603 (2009).
[17] J. F. Zhou, T. Koschny, and C. M. Soukoulis, Opt. Express **16**, 11147 (2008).
[18] S. Zhang *et al.*, Opt. Express **14**, 6778 (2006).
[19] J. Valentine *et al.*, Nature (London) **455**, 376 (2008).
[20] V. P. Drachev *et al.*, Opt. Express **16**, 1186 (2008).
[21] C. E. Kriegler *et al.*, IEEE J. Sel. Top. Quantum Electron. **16**, 367 (2010).
[22] C. Rockstuhl *et al.*, Phys. Rev. B **77**, 035126 (2008).
[23] S. Xiao *et al.*, Nature (London) **466**, 735 (2010).